IEEE Access
Multidisciplinary | Rapid Review | Open Access Journal

Received 14 September 2023, accepted 3 October 2023, date of publication 5 October 2023, date of current version 18 October 2023.

Digital Object Identifier 10.1109/ACCESS.2023.3322205

RESEARCH ARTICLE

Enhancing Medical Image Reclamation for Chest Samples Using B-Coefficients, DT-CWT and EPS Algorithm

B. P. PRADEEP KUMAR[1], PRAMOD K. B. RANGAIAH[2], (Member, IEEE), AND ROBIN AUGUSTINE[2], (Member, IEEE)

[1]Department of Electronics and Communication Engineering, HKBK College of Engineering, Bengaluru 560045, India
[2]Division of Solid State Electronics, Microwaves in Medical Engineering Group, Department of Electrical Engineering, Uppsala University, 75103 Uppsala, Sweden

Corresponding authors: Robin Augustine (Robin.Augustine@angstrom.uu.se) and Pramod K. B. Rangaiah (pramod.rangaiah@angstrom.uu.se)

This work was supported in part by the following projects: ''AI-based Detection of Acute Respiratory Distress Syndrome (AI-DARDS)'', Dr. no. 2020–03612, Indo-Swedish-Vinnova project, Swedish SSF Projects ZeroIoT (CH10-0003), Wireless Brain-Connect inteRfAce TO machineS: B-CRATOS, European Union's Horizon 2020 Research and Innovation Program, Grant agreement ID: 965044, DOI. 10.3030/965044, Funded under EXCELLENT SCIENCE-Future and Emerging Technologies (FET) Open, Coordinated by UPPSALA UNIVERSITET, Sweden. Start date 1 March 2021 and End date 28 February 2025.

ABSTRACT This paper introduces a novel approach for medical image reclamation, specifically focusing on enhancing chest image resolution. The proposed method introduces the Dual-Tree Complex Wavelet Transform (DT-CWT) with Edge Preservation Smoothing (EPS) filters to balance visual clarity. The resulting Image Reclamation system maintains high-quality results while preserving image edges. Performance validation using established metrics like Peak Signal-to-Noise Ratio (PSNR), Structural Similarity Index (SSIM), Root Mean Square Error (RMSE), and entropy demonstrates substantial improvements: PSNR of 31, SSIM of 0.99, RMSE of 8.25, and entropy of 1.03. Furthermore, the algorithm extracts features from the enhanced chest image through symlet transform, allowing for Bhattacharya coefficient computation and unique bin analysis to enhance image retrieval. Experimental results show efficiency gains, increasing the top 5 matching images' retrieval score from 320 to 512. This approach promises to enhance medical image reclamation in emergency settings, facilitating quicker and more accurate diagnoses and treatments for acute chest injuries. Ultimately, this work can potentially save lives, reduce complications, and improve patient outcomes in chest trauma emergencies.

INDEX TERMS Medical image reclamation, image resolution enhancement, dual-tree complex wavelet transform (DT-CWT), chest visual-based image reclamation (Chest VBIR), edge preservation smoothing (EPS) filter.

I. INTRODUCTION

In recent years, the landscape of medical imaging has been reshaped by the fusion of pioneering technologies and computational breakthroughs [1]. The imperative to adeptly distill, analyze, and retrieve crucial insights from medical images has become paramount for precise diagnostics and effective patient management [2]. Amidst this evolution, one intricate realm that stands out is the domain of chest radiological images [3]. Within this domain, the precise retrieval of images and the extraction of pertinent features emerge as cornerstones, aiding medical practitioners in making well-informed clinical assessments [4]. In scenarios demanding swift medical decisions, particularly in emergency situations, the role of junior doctors can be pivotal. However, challenges in experience and expertise can sometimes hinder optimal judgment [5]. This system holds the potential to save lives by offering invaluable references that align with the current patient scenario.

Medical image reclamation, the process of retrieving relevant images from unannotated image databases, plays a pivotal role in modern healthcare and research applications

The associate editor coordinating the review of this manuscript and approving it for publication was Mohammad Zia Ur Rahman.

[6]. Accurately and efficiently retrieving medical images is essential for diagnosis, treatment planning, and medical research. However, the vast and dynamic collections of medical images pose significant challenges in identifying meaningful and pertinent images [7]. A novel approach using the Bhattacharyya coefficient as a similarity measure has emerged as a promising solution to address this issue.

In recent years, the Bhattacharyya coefficient has gained popularity as an effective statistical measure to assess the similarity between probability distributions [8]. Its application in medical image reclamation has shown considerable potential in overcoming the discrepancy between high-level semantic concepts used by researchers and low-level visual features extracted from images for indexing [9]. Despite the exponential growth in data, content-based image reclamation remains a challenging task [10]. Image reclamation is crucial for various applications such as crime prevention, biodiversity, information systems, historical research, fingerprint identification, and medicine [11]. Typically, three techniques are employed for image reclamation: semantic-based, text-based, and content-based [12]. Given the increasing demand for content-based image reclamation in digital libraries, military operations, education, and architectural design, it has become a highly active area of research in recent years [13]. Traditional database technology faces difficulties in handling the reclamation of large data volumes, as conventional text-based databases do not adequately address the requirements of image databases [11]. In the past, image reclamation relied on textual annotation, where images were interpreted with text and then retrieved from a database that primarily focused on textual information rather than visual features for searching images [14].

Customary image reclamation methods face limitations in terms of efficiency and resource utilization, driving the development of new technologies [15]. Many conventional approaches rely on adding metadata to images, such as descriptions, keywords, and captions, to facilitate reclamation [16]. However, the manual labor involved in associating keywords with images for textual annotation is unable to capture the diverse and ambiguous nature of image content [17]. Content-Based Image Reclamation (CBIR) systems aim to enhance reclamation accuracy by focusing on salient image features. These systems analyze image characteristics to provide more precise and relevant search results. Nonetheless, most CBIR methods utilize only one or two feature descriptors, leading to lower accuracy. For example, the widely used SIFT (Scale-Invariant Feature Transform) descriptor is effective in cluttered environments but struggles with low illumination and poorly located key points, which hampers CBIR performance. This study employs pre-trained deep learning models to extract prominent features and improve CBIR outcomes. CBIR revolves around searching based on image content rather than relying on metadata like descriptions, keywords, and tags [18]. CBIR was introduced in the 1990s to address the limitations of labor-intensive text-based image reclamation systems [19]. It enables the extraction or reclamation of visually similar image content from extensive databases, significantly reducing reclamation time compared to cumbersome and unstructured browsing methods [20]. The visual content of images is stored as feature vectors retrieved from the database [17].

Numerous research papers and reports have extensively explored various image resolution enhancement techniques and algorithms to improve image resolution and peak signal-to-noise ratio (PSNR). Among these techniques, the wavelet domain approach based on complex wavelet transforms has emerged as a powerful tool for resolution enhancement. Varish et al. [21] proposed a resolution enhancement scheme using a dual-tree complex wavelet transform (DT-CWT). This approach involves decomposing a satellite input image into high-frequency sub-bands using DT-CWT, which is nearly shift-invariant. The interpolated high-frequency sub-bands, along with the low-resolution input image, are then combined using inverse DT-CWT, resulting in a resolution-enhanced image. Objective and subjective analyses have demonstrated the superiority of this method over conventional and state-of-the-art techniques. Similarly, Selwin et al. [22] introduced a satellite image resolution enhancement technique based on discrete wavelet transform (DWT) and interpolation of high-frequency sub-bands. An intermediate stage, employing stationary wavelet transform (SWT), enhances image edges, leading to sharper results. The evaluation of satellite benchmark images validated the effectiveness of this approach, surpassing conventional and state-of-the-art image resolution enhancement techniques in terms of quantitative and visual measures. Furthermore, Gawande et al. [23] presented the design and implementation of various orthogonal and bi-orthogonal rational-coefficient wavelet filters, satisfying the Hilbert transform pair condition and other desirable properties. These filters were shown to achieve excellent energy compaction, wavelet smoothness, and directionality without significant loss due to rational-coefficient constraints.

In a structured Visual-based Image Reclamation (VBIR) system, visual attributes such as color, shape, texture, and spatial information are automatically extracted from each image in the database, as shown in Figure 1. These attributes are stored in a feature database, representing a compact fixed-length real-valued multipart feature vector or signature for each image. Compared to the image data, the size of the feature data for each visual characteristic is significantly smaller.

To use the VBIR system, the user prepares a query image and submits it to the system [24], [25]. The system extracts the visual properties of the query image in the same way as it does for the images in the database. It then identifies images in the database whose feature vectors closely match those of the query image and sorts them based on their similarity values. The system operates on less compact feature vectors, making VBIR fast, efficient, and superior to text-based reclamation.

A VBIR system offers two main applications: precise image matching, where a query image is compared to an

image in the database, and approximate image matching, where the system identifies the most closely matched images to the query image [26]. VBIR's effectiveness relies on extracting informative features from the visual characteristics of the images [27].

In the past, image reclamation systems relied on textual descriptions for organizing images. In an ideal VBIR system, a database represents images as multi-dimensional feature vectors. Users input sample images or sketches, which are converted into feature vectors. The system then uses an indexing scheme to calculate similarities/differences between query vectors and database vectors for efficient searching. To overcome the challenge of high-dimensional feature vectors, dimensionality reduction techniques like PCA (Principal Component Analysis) are commonly employed. PCA maps the data onto a lower-dimensional subspace, capturing the most significant variations for effective indexing and retrieval. PCA technique reduces the dimensionality of a feature vector X by projecting it onto a lower-dimensional subspace represented by V: $Y = X \cdot V$, where Y is the reduced feature vector and V contains the eigenvectors corresponding to the top principal components.

This paper presents an in-depth exploration of the Image Reclamation system utilizing the Bhattacharyya coefficient. The proposed approach involves the decomposition of query images using the DT-CWT and the application of the Edge preservation smoothing (EPS) filter. The proposed Image Reclamation system leverages the benefits of the DWT algorithm to extract essential features from query input medical images, enabling enhanced resolution and improved retrieval accuracy. By leveraging these techniques, the resolution of query medical images is enhanced, leading to improved reclamation rates. The proposed Image Reclamation system incorporates the DWT algorithm, a powerful technique utilized for dimensionality reduction and feature extraction in medical image processing. DWT decomposes the input image into four sub-bands: LL, LH, HL, and HH [28]. The LL sub-band represents the approximate image with low-frequency components, serving as the foundation for further decomposition. The LH sub-band captures horizontal features, while the HL sub-band highlights vertical features. Lastly, the HH sub-band extracts diagonal features, collectively contributing to an efficient and comprehensive representation of medical images for accurate retrieval.

The primary objective of this study is to improve the image quality by analyzing various metrics, i.e., PSNR, Structural Similarity Index (SSIM), Root Mean Square Error (RMSE), and Entropy. We further analyze the impact of the effectiveness of the Bhattacharyya coefficient in accurately identifying and retrieving relevant medical images from large unannotated databases using a similarity score.

To validate the proposed approach, we considered 26 untrained image samples labeled as A to Z with improved resolution levels. Extensive experiments are conducted on a dataset of 60 trained chest samples. The results demonstrate the superiority of the Bhattacharyya coefficient in achieving precise and efficient medical image reclamation. The obtained outcomes highlight the potential of this approach in advancing medical image retrieval for improved diagnosis and research outcomes.

Although the field of chest imaging has seen considerable work, this research adds distinct value. It integrates advanced signal processing techniques (DT-CWT and EPS) for unique applications in enhancing chest X-ray image quality. Rigorous quantitative assessments using statistical parameters provide objective evaluation metrics. Efficient image retrieval via Battacharya Coefficients and DT-CWT improves access to relevant medical images. In summary, while the chest imaging field is well-established, this research brings novel applications, rigorous assessments, and improvements, offering valuable contributions.

A. SIGNIFICANT CONTRIBUTIONS

This research paper makes several significant contributions to the field of medical image processing and analysis:

- Integration of Cutting-Edge Techniques: Incorporates DT-CWT and EPS algorithms to enhance chest X-ray image quality.
- Robust Quantitative Evaluation: Utilizes statistical parameters, including Entropy, SSIM, PSNR, and RMSE, for objective assessment of image quality improvement.
- Efficient Image Retrieval: Enhances image retrieval using Battacharya Coefficients and 2D-DWT, simplifying access to relevant medical images.
- Impressive Experimental Results: Conducts extensive experiments on a dataset of 60 chest X-ray samples, achieving high PSNR (31), SSIM (0.99), low RMSE (8.25), and minimal entropy (1.03), demonstrating the effectiveness of the proposed approach.
- Enhanced Retrieval Score: Increases the retrieval score for the top 5 matching images from 320 to 512, emphasizing practical utility for medical image analysis and diagnosis.

In summary, this research paper represents a substantial contribution to the field of medical image processing. It offers advanced techniques for enhancing chest X-ray images and significantly improves image retrieval efficiency, ultimately enhancing the quality of medical image analysis and diagnosis.

The organization of this article is as follows: Section II presents a detailed literature review, focusing on the techniques in image reclamation and the utilization of DWT and interpolation methods in the reclamation system. Moving on to Section III, we present a novel framework aimed at enhancing medical images using a combination of DT-CWT and EPS algorithms. The primary goal of this framework is to facilitate reclamation in the chest VBIR method, employing Battacharya Coefficients for improved performance. This section includes a data flow diagram, process flow chart, and pseudocode to provide a comprehensive understanding

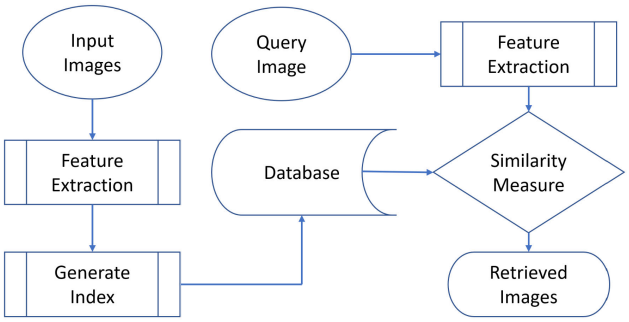

FIGURE 1. General system architecture for image reclamation which provides an overview of the system's structure.

of the proposed approach. Section IV discusses the results obtained from the experiments, accompanied by visual comparisons and quantitative measurements. These results serve to demonstrate the effectiveness and performance of the proposed method. Finally, in Section V, the article concludes with a summary of the findings and potential future research directions, outlining the contributions and implications of the study. To offer more in-depth insights, the Appendix in Section V contains supplementary information, including detailed algorithm parameters and evaluation results, further enriching the reader's understanding of the proposed approach.

II. RELATED WORK

Image reclamation in medical imaging has become a pivotal area of research aimed at enhancing image quality and resolution for improved diagnostic accuracy. This comprehensive literature review presents a survey of key studies on image reclamation, highlighting the latest advancements and approaches in the field, Liu et al. [29] proposed a robust medical image reclamation approach using VBIR technique with DT-CWT and EPS filter. Their method demonstrated remarkable results in enhancing medical images' resolution and visual quality, highlighting the efficacy of DT-CWT and EPS filters in image reclamation tasks. Sharma et al. [30] delved into multi-scale patch-based image reclamation using convolutional neural networks. Their research showcases the advancements in deep learning techniques for medical image analysis and reclamation, opening new avenues for precise and automated image enhancement.

Wen et al. [31] proposed spectral-based CT image reclamation using total variation minimization. This approach introduces a novel and effective method for image enhancement in medical imaging, promising for lung image reclamation. Ahmad et al. [32] investigated image reclamation in lung CT scans using deep learning methods. Their work contributes to the growing body of literature on deep learning applications in medical imaging, emphasizing the potential of these techniques in lung image reclamation. Rangaiah et al. [33] conducted a study on the dielectric characterization and statistical analysis of ex-vivo burnt human skin samples for microwave sensor development. Although not directly related to image reclamation, this research provides insights into the dielectric properties of biological tissues, potentially applicable to medical image reclamation [34]. Melek et al. [35] investigated a novel wavelet-based approach for image reclamation using dual-stage sparse representation. This study offers a unique perspective on sparse representation techniques, which can potentially enhance the efficiency of medical image reclamation.

Zheng et al. [36] introduced a multi-scale and multi-task deep neural network for image reclamation, achieving significant improvements in image quality and resolution. Kiruban et al. [37] developed an image reclamation approach using adaptive thresholding and deconvolution to enhance medical images with reduced noise and improved visual clarity. Liu et al. [38] introduced parallelized container-based quantization techniques for enhanced medical image reclamation on the cloud. This study presents efficient strategies for processing large medical image datasets, enabling faster and scalable image reclamation processes. Sankar et al. [39] presented a technique for single-image haze reclamation using the dark channel prior. Though not directly related to medical imaging, this study provides valuable insights into general image enhancement methods, which can potentially be adapted for medical image reclamation. In another study by Rangaiah et al. [34], the authors explored clustering techniques for dielectric and color profiles of ex-vivo burnt human skin samples. While focused on burnt skin samples, these clustering methods hold the potential for image reclamation and analysis of medical images. Kamble et al. [40] proposed a robust reclamation system using a supervised classifier that focuses on isolated features. Grain topographies were mined using the gray-level co-occurrence environment algorithm. The dataset was classified into three classes: normal, benign, and malignant, and the query image was classified to a specific class to retrieve relevant images from the database.

Li et al. [29] proposed a deep learning-based generative adversarial network (GAN) approach for image reclamation, showcasing its ability to generate high-resolution medical images with enhanced visual quality. Using Gaussian mixture models, Liu et al. [41] proposed a nonlocal patch-based image reclamation approach. Their research emphasizes the significance of nonlocal information in improving image reclamation outcomes, providing valuable insights for medical image processing. Prasenan et al. [42] presented an adaptive fuzzy histogram equalization-based image reclamation technique, demonstrating its effectiveness in enhancing medical images with varying contrast levels.

Javaheri et al. [43] presented an adaptable and cost-effective architecture for parallelizing container-based quantization techniques to obtain the best possible quantized image on the cloud. The approach is scalable and can be applied to large datasets efficiently. The quantization methods employed in this study include fuzzy entropy and genetic algorithm-based techniques, utilizing different types of membership functions to calculate the fuzzy entropy. The optimal quantized image is determined using the

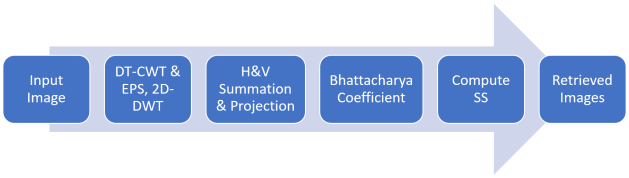

FIGURE 2. Proposed chest VBIR method through utilization of B coefficients design of the model.

SSIM, resulting in superior outcomes compared to the traditional serial approach. This research contributes to the field of image quantization, providing a cost-effective and parallelized solution for processing large-scale image datasets, which has potential applications in various image processing and analysis tasks. Thakur et al. [44] explored a non-local structure tensor-based image reclamation method for preserving edges and enhancing texture details in medical images. Antoni et al. [45] introduced the Red Fox Heuristic Optimization Algorithm (RFOA) to enhance heuristic operations in two-dimensional image analysis. This involved modifying equations and introducing a novel fitness function, ultimately automating threshold selection by converting selected pixels to black or white. This tailored approach for image analysis was complemented by Dawid Połap et al. [46], who developed the Red Fox Optimization Algorithm (RFO) based on a combination of local and global optimization methods, complete with a reproduction mechanism. Their innovative optimization model underwent benchmark tests, encompassing 22 test functions and addressing seven classic engineering optimization problems. The experimental results were thoughtfully compared with other meta-heuristic algorithms, highlighting the potential advantages of this comprehensive approach.

The field of visual-based reclamation from unannotated image databases presents a dynamic and versatile research domain, with challenges that vary based on factors such as domain of interest, database size, and prior knowledge availability. While retrieving iconic images from well-defined contexts may be straightforward, the task becomes considerably more challenging when dealing with vast and heterogeneous collections of images, as found on the World Wide Web. In the context of VBIR, a significant challenge arises from the discrepancy between high-level semantic concepts used by humans to interpret visual information and low-level visual features employed by computers for image indexing. This paper explores two critical research themes in VBIR: (1) the identification of relevant features and determination of their similarity, and (2) the development of effective indexing strategies for presenting images to users. Several research articles, including those by Mary et al. [47] and Tyagi et al. [48], have contributed to the advancement of techniques and methodologies in this rapidly evolving field.

III. THE PROPOSED VISUALIZING SOLUTIONS

This section describes the required system architecture for the Enhancing Medical Image Reclamation system. In Figure 2

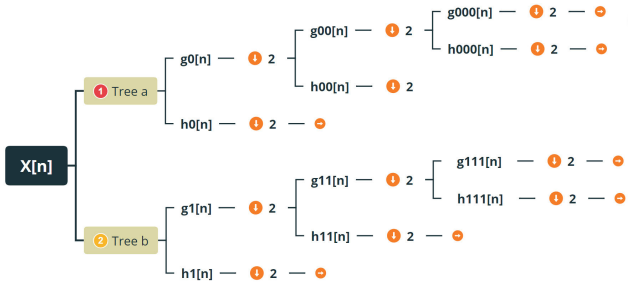

FIGURE 3. Tree diagram illustrating the dual-tree complex wavelet transform (DT-CWT) Filters g0[n] and g1[n].

illustrates the chest VBIR Method using Battacharya Coefficients and DT-CWT EPS Algorithm for creating an adaptable digital image reclamation system to effectively manage large-scale chest X-ray images. MATLAB is the chosen software tool for implementing this framework. The aim of this proposed approach is to create a scalable digital image reclamation system using the VBIR method. The main objectives are as follows: Conduct a comprehensive review of the existing literature to evaluate the effectiveness of techniques used for mitigating X-ray segmentation issues using image VBIR. This will help in identifying research gaps and open issues that need to be addressed. Implement the discrete wavelet transform to obtain the quantities and determine the flat, perpendicular summation and prognose of the images. Utilize the Battacharya coefficient to retrieve similar images in the VBIR method. The complete process has been particularized in the following sub-sections.

The DT-CWT is an advanced signal processing technique that generates complex coefficients using two separate trees, resulting in both real and imaginary parts. This process yields eight sub-bands in total: two complex-valued low-frequency sub-bands and six high-frequency sub-bands. DT-CWT is an enhancement of the DWT and is known for its superior directional selectivity (Equation 1). The DWT decomposes an image $I(x, y)$ into approximation (LL) and detail sub-bands (LH, HL, HH) at different scales j and positions n. It combines the desirable properties of both the DWT and the Continuous Wavelet Transform (CWT), such as approximate shift invariance and excellent directional selectivity. Figure 3 shows the tree diagram: g0[n] and g1[n] is the set of real-valued sub-band images of two trees, and h0[n] and h1[n] are the set of imaginary sub-band images of two trees. The g0[n] filter serves as the analysis low-pass filter, skillfully extracting the input signal's low-frequency components or approximation coefficients. It applies a smoothing operation, effectively preserving the coarse details and overall structure of the signal. Its design is meticulously optimized for excellent frequency response with minimal passband ripple. On the other hand, the g1[n] filter functions as the analysis high-pass filter, capturing the high-frequency components or detail coefficients of the input signal. It excels at detecting fine details and sharp edges in the image, demonstrating high sensitivity to signal changes. Its design is tailored to prioritize

responsive high-frequency behavior.

$$\left.\begin{aligned} I_j(x,y) &= \sum(I(x,y), \phi_{j,n}(x,y)) \\ H_{j,n}(x,y) &= \sum(I(x,y), \psi_{j,n}(x,y)) \end{aligned}\right\} \quad (1)$$

where $\phi_{j,n}(x,y)$ and $\psi_{j,n}(x,y)$ are the scaling and wavelet functions at scale j and position n.

The DT-CWT produces complex coefficients by employing dual trees to generate both real and imaginary parts. This results in two complex-valued low-frequency sub-bands and six high-frequency sub-bands. DT-CWT is a variation of the DWT that uses two separate trees of complex wavelets to achieve better directional selectivity. The DT-CWT of an image $I(x,y)$ can be represented as $DT-CWT(I(x,y)) = DT-CWT_{real}(I(x,y)) + i.DT-CWT_{imag}(I(x,y))$, where $DT-CWT_{real}(I(x,y))$ and $DT-CWT_{imag}(I(x,y))$ represent the real and imaginary components of the DT-CWT.

To ensure invariance and minimize artifacts during reconstruction, DT-CWT combines the outputs of these two trees. Notably, the high-frequency sub-bands produced by directional selective filters exhibit peak magnitude responses at specific orientations, such as 75, 45, and 15 degrees. This orientation sensitivity enables the detection of features and their orientations within the image, which is valuable for tasks like edge detection and linear feature identification. The DT-CWT technique employs Lanczos interpolation to further enhance edge detection and linear feature identification. This process involves mapping each input image pixel to a translated and scaled copy of the Lanczos kernel. The scaling factor is represented by the parameter "beta". This process maps each input image sample to a translated and scaled copy of the Lanczos kernel (Fourier kernel with a 4×4 input cell). The filter reconstruction kernel, denoted as L $L(x)$ (Equation 2), plays a crucial role in this interpolation step.

$$L(x) = \left\{\begin{array}{cc} 1 & if\ x = 0 \\ \frac{a\ sin(\pi x)\ sin(\frac{\pi x}{a})}{(\pi x)^2} & if\ 0 < |x|\ a \\ 0 & otherwise \end{array}\right\} \quad (2)$$

Following the DT-CWT and interpolation steps, the EPS technique is applied. EPS leverages a Gaussian low-pass filter to preserve essential image features, particularly edges while reducing noise. The mathematical representation of $EPS(I(x,y)) = I(x,y) * G_\sigma(x,y)$, where $G_\sigma(x,y)$ is the 2D Gaussian kernel with standard deviation σ. After the EPS algorithm, several statistical quality parameters are employed to assess the quality of the enhanced image. These parameters offer valuable insights into the effectiveness of the image enhancement process: The entropy H of an image $I(x,y)$ is a measure of the amount of information or uncertainty in the image's pixel values and is computed as shown in the Equation 3:

$$H(I) = -\sum_{x,y} p(I(x,y)) \cdot log_2(p(I(x,y))) \quad (3)$$

where, $p(I(x,y))$ is the probability distribution of pixel values in the image. SSIM is a measure of the structural similarity between two images and can be explained as shown in the Equation 4

$$SSIM(I_1, I_2) = \frac{(2 \cdot \mu_1 \cdot \mu_2 + C_1) \cdot (2 \cdot \sigma_{12} + C_2)}{(\mu_1^2 + \mu_2^2 + C_1) \cdot (\sigma_1^2 + \sigma_2^2 + C_2)} \quad (4)$$

where, μ_1 and μ_2 are the means of the two images, σ_1^2 and σ_2^2 are their variances, σ_{12} is their covariance, and C_1 and C_2 are constants to stabilize the division. PSNR and RMSE are commonly used metrics to quantitatively evaluate the quality of image enhancement or restoration processes. Higher PSNR values and lower RMSE values indicate better image quality and closer similarity between the original and processed images. PSNR measures the quality of an image by calculating the ratio of the maximum possible pixel value to the mean squared error (MSE) between the original image I and the processed image $\hat{I}$. This can be defined as shown in Equation 5

$$PSNR = 10 \cdot log_{10}(\frac{255^2}{MSE}) \quad (5)$$

where 255 is the maximum pixel value (for an 8-bit image) and $MSE = \frac{1}{N}\sum_{i=1}^{N}\left(I(i) - \hat{I}(i)\right)^2$ is the mean squared error, and N is the total number of pixels. $RMSE = \sqrt{MSE}$ measures the average magnitude of the differences between corresponding pixel values in the original image I and the processed image $\hat{I}$.

DT-CWT, interpolation, and EPS contribute to image enhancement, followed by the analysis of statistical quality parameters. These parameters collectively provide insights into the quality of the enhanced image, helping to gauge the success of the image. The aim is to maximize SSIM and PSNR while minimizing Entropy and RMSE to achieve high-quality results.

A. PROPOSED VBIR DATA FLOW DIAGRAM (DFD)

DFD is a visual approach to illustrate the system's process flow. During the initial analysis stage, a model is used to represent how data is processed and moves through the system. The models consist of core processes, data stores, and data flows between various models. This technique is employed to demonstrate how data will pass through a series of processing levels or steps.

Figure 4 depicts a Level-0 DFD that illustrates the primary process involved in the chest VBIR method 1. This process takes a query X-ray chest image and utilizes a Visual-based image reclamation technique to process it into the resulting retrieved image.

The Level-1 Data Flow Diagram, depicted in Figure 4, represents a detailed breakdown of the Level-0 DFD, revealing the primary process 1 followed by three sub-processes: the 2D-DWT process {1.1}, the application of the VBIR method {1.2}, and the reclamation of the resulting image {1.3}.

Level-1.1 DFD in Figure 4 depicts to provide a more in-depth view of the 2D-DWT technique {1.1}. This process involves the computation of approximation quantities, such

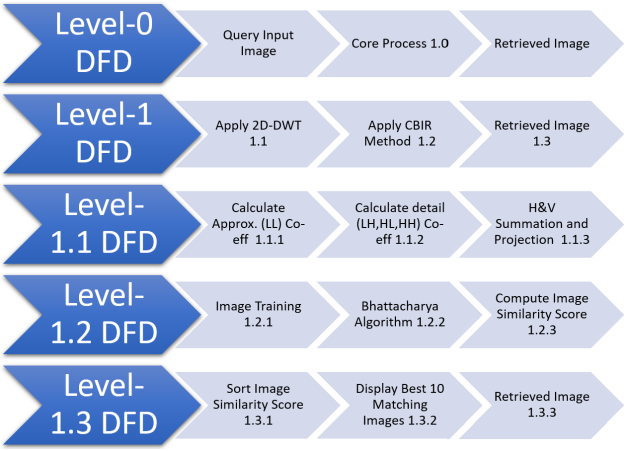

FIGURE 4. Evolution from Level-0 DFD to Level 1.3 DFD in the System design.

as the LL coefficient elements {1.1.1}, from digitized X-ray chest images. The remaining detail quantities, including LH, HL, and HH coefficients, are also computed and stored in vectors {1.1.2}. Furthermore, the generation of flat summation, perpendicular summation, flat prognose, and perpendicular prognose is conducted at this stage, which will be displayed {1.1.3}.

In Figure 4, the Level-1.2 Data Flow Diagram presents a detailed perspective of the VBIR process. During VBIR, robust multi-dimensional features are identified from the input sample chest image and projected onto binary codes. Subsequently, image training {1.2.1} is performed, followed by the application of the Bhattacharya coefficient algorithm {1.2.2} to establish similarity scores for each sample in the image catalogue. This algorithm calculates the similarity score for each image data, which is crucial for the image reclamation process.

Figure 4 showcases the Level-1.3 Data Flow Diagram, demonstrating the breakdown of the Reclamation of Image {1.3} process. This process is further decomposed into three subprocesses: sorting image similarity scores {1.3.1}, displaying the top 5 matching images {1.3.2}, and enhancing retrieval images based on the best similarity scores and Bhattacharya score {1.3.3}. These meticulously designed steps are indispensable for effective and efficient image reclamation, particularly in biomedical imaging applications and other research domains. The flat projection (FP) of an image $I(x, y)$ is based on the column-wise sum vectors, i.e., $FP(x) = \sum_y I(x, y)$, and the perpendicular projection (PP) is based on row sum vectors, i.e., $PP(y) = \sum_x I(x, y)$. The prognose function computes derivatives of a projection vector P at a particular index i using the formula $Prognose(P, i) = P(i + 1) - P(i)$.

B. ENHANCED IMAGE RECLAMATION ALGORITHM USING BHATTACHARYA COEFFICIENTS

The presented data flow diagrams provide a scientifically rigorous representation of the image reclamation system, offering valuable insights into the underlying processes and

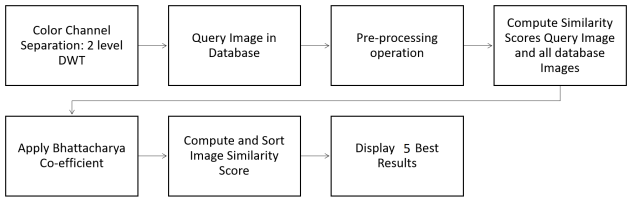

FIGURE 5. Algorithmic treasure map of the proposed system.

methodologies involved in the image reclamation procedure. In medical imaging, segmentation presents several challenges, such as Additive white Gaussian noise (AWGN), occlusion during capturing, scanning articles, low contrast, and tissue distortion. Therefore, the interpolation method is selected in such a way as to provide approximate shift invariance and excellent directional selectivity for the input images. Then, an enhanced chest image sample is taken as input, and its features are extracted. Figure 5 depicts the process flow chart of the proposed technique. We integrate a chest atlas model into the system to provide previous knowledge for better reclamation. In order to determine a statistical model for each patient's X-ray, our system first identifies the most similar images from a training set of images (atlases), then uses a non-rigid registration algorithm to deform those training atlases into the patient's CXR [24].

The proposed system employs the DWT algorithm to reduce dimensionality and perform feature extraction from images. The DWT decomposes the image into four sub-bands (sub-images): LL, LH, HL, and HH. The LL sub-band contains the approximate image of the input image and represents the low-frequency sub-band, which is used for further decomposition. The LH sub-band extracts horizontal features of the original image, the HL sub-band provides vertical features, and the HH sub-band gives diagonal features. This decomposition process enables the extraction of meaningful features for similarity assessment and reclamation.

The image prognoses (H1, H2) and prognose bins (bins1,bins2) are essential for feature extraction and similarity calculation in the Image Prognoses and Summation process. The summation along rows (Sr0) and columns (Sc0) of the database images Itemp is computed to derive meaningful pattern representations. The summation process enhances the ability to capture relevant patterns and characteristics for comparison. The intersection operation plays a crucial role in identifying the shared characteristics between the query image and the database images, aiding in the retrieval of relevant images. To obtain the intersection (Q) of $bins2$ and $bins20$, which corresponds to the common elements between the two sets of bins, we use the following Equation 6

$$Q = bins2 \cap bins20 \tag{6}$$

where q represents the set of common elements. The value of alpha ($\alpha = \frac{n}{n+m}$), representing the relative contribution of P and Q. Where n and m are the lengths of P and Q, respectively. Alpha (α) is used to balance the impact of the unique bins (P) and the intersection (Q) when computing the BC, ensuring a

comprehensive similarity score. This balancing step prevents any one feature from dominating the similarity calculation and enhances the robustness of the reclamation system.

The Bhattacharyya coefficient (BC) is a statistical measure used to quantify the similarity between two probability distributions, P and Q, given by Equation 7

$$BC = \sum_{i=1}^{n} \sqrt{P(i).Q(i)} \tag{7}$$

where n is the number of unique bins in the distributions. The image reclamation process involves finding the top 5 matching images from the database based on the highest Bhattacharyya scores (BCi). This is achieved using the following Equation 8.

In the context of image reclamation, the BC is employed to assess the resemblance between the feature vectors of the query image and the images stored in the database. It serves as a critical similarity measure for image retrieval, ensuring accurate matches for the given query image.

$$Top\ 5\ Matching\ Images = \sum(BCi) \tag{8}$$

where $argmax_i$ returns the indices of the top 5 maximum values of BCi. These top matching images represent the best reclamation outcomes for the given query image, providing valuable insights for medical diagnosis and research applications.

The provided pseudo-code represents the algorithm for training the reclamation system. It outlines the steps involved in processing the query image and the images in the database, computing Bhattacharya coefficients, and determining the top 5 matching images based on similarity scores. The algorithm aims to enhance image reclamation performance by calculating and comparing key features of the query image with images in the database.

Display the database image score and Bhattacharya score. After completing the loop for all images in the database, find the top 5 matching images and stop. In the Appendix, we present the pseudocode and detailed explanation of the wavelet-based decomposition algorithm used in the image pre-processing. The algorithm leverages the DWT to decompose the input image into its approximation and detail coefficients at multiple resolution levels. We provide a step-by-step breakdown of the algorithm, including the process of retrieving approximation and detail coefficients for each level of decomposition. Additionally, the implementation of interpolation methods, such as nearest neighbor, bilinear filtering, and bi-cubic interpolation, for image quality enhancement is thoroughly described. These techniques play a crucial role in various image pre-processing applications, and their detailed explanation in the appendix enhances the understanding of the proposed methodology.

Algorithm 1 Image Reclamation Using Bhattacharya Coefficient

I (query image), $bins2$, $H2$, $bins1$, $H1$, Sc, Sr (database) **Data:** Load the database of images and their corresponding feature vectors $H1$, $H2$, $bins1$, $bins2$, Sc, and Sr.
Data: Select the query image, I, for image reclamation.
foreach *image i in the database* **do**
  $H10 \leftarrow H1(i)$;
  $Bins10 \leftarrow bins1(i)$;
  $H20 \leftarrow H2(i)$;
  $Bins20 \leftarrow bins2(i)$;
  $Itemp \leftarrow$ database image i;
  $Sr0 \leftarrow$ Summation along rows of $Itemp$;
  $Sc0 \leftarrow$ Summation along columns of $Itemp$;
  $P \leftarrow$ Unique bins in the query image;
  Generate respective bins for the database image:
  $Q \leftarrow$ Intersection of $bins2$ and $Bins20$;
  $n \leftarrow$ length(P);
  $m \leftarrow$ length(Q);
  $Alpha \leftarrow n/(n+m)$;
  Initialize temporary variables: $p\_temp \leftarrow 0$, $q\_temp \leftarrow 0$;
  foreach *bin x in P* **do**
    $p\_temp \leftarrow p\_temp + \sqrt{p1(x) \cdot p2(x)}$;
  end
  foreach *bin y in Q* **do**
    $q\_temp \leftarrow q\_temp + \sqrt{q1(y) \cdot q2(y)}$;
  end
  $BC \leftarrow Alpha \cdot p\_temp + (1 - Alpha) \cdot q\_temp$;
  $BCi(ii) \leftarrow$ round(BC) // Store BC score for this database image
  Display(database image i score);
  Display('Bhattacharya score');
end
Select the top 5 database images with the highest Bhattacharya scores as the matching images for the query image.

IV. RESULTS AND DISCUSSIONS

This section presents the outcomes achieved through anticipated enhanced VBIR techniques. Figure 6 showcases the untrained input query image used in the model. The dataset of chest radiological images has been carefully organized and stored in the catalogue folder, with particular attention to the feature set of the collected samples. Our approach aims to enhance the resolution process by matching relevant regions of interest in chest radiological images.

Figure 7 illustrates a bar graph evaluating the performance of various interpolation algorithms that enhance the resolution of untrained input query images. The algorithms under consideration include the nearest neighbor, bilinear filtering, bicubic interpolation, DT-CWT, and DT-CWT & EPS. The graph presents the PSNR values, which indicate image quality. Among these algorithms, the "DT-CWT & EPS" algorithm stands out with the highest PSNR value, reaching 30.07 dB, as represented by the blue-colored bars in the

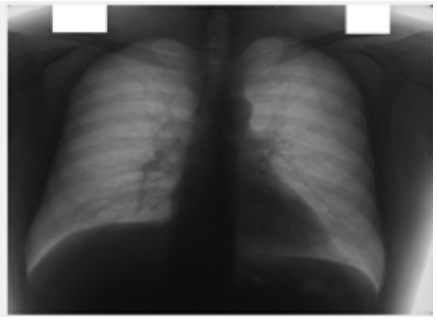

FIGURE 6. Explore the intricacies of image A from the database.

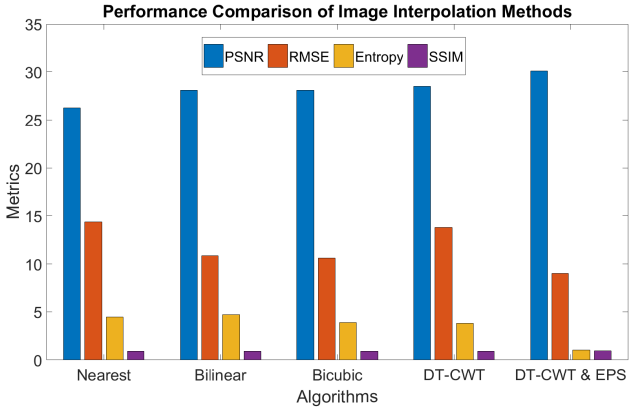

FIGURE 7. Assessing interpolation algorithm performance input query image A.

graph. This exceptional PSNR value indicates superior image quality. Additionally, ''Bilinear'' and ''Bicubic'' perform admirably with PSNR values of 28.08 dB and 28.11 dB, respectively, showcasing their effectiveness. On the other hand, ''Nearest'' and ''DT-CWT'' exhibit lower PSNR values and the RMSE. Notably, the ''DT-CWT & EPS'' algorithm boasts the lowest RMSE value at 9.006, signifying greater accuracy. In contrast, ''Bilinear'' and ''Bicubic'' display reasonable RMSE values of 10.87 and 10.62, respectively, while ''Nearest'' and ''DT-CWT'' show relatively higher errors, as indicated by the orange-colored bars in the graph. Furthermore, the graph uses color coding to represent entropy values, where the ''DT-CWT & EPS'' algorithm achieves the lowest entropy value at 1.031. This low entropy value implies better image compression and more efficient information representation. ''Bicubic'' follows as the second-lowest in terms of Entropy at 3.88, while ''Nearest'' registers the highest entropy value at 4.70, represented by the yellow bar. Finally, the violet-colored bars in the graph represent the SSIM. Again, the ''DT-CWT & EPS'' algorithm attains the highest SSIM value of 0.97, indicating superior structural similarity in comparison, ''Nearest'' and ''Bicubic'' exhibit slightly lower SSIM values at 0.91 and 0.92, respectively.

Figure 8 displays the results of resolution enhancement for 26 untrained query images using the DT-CWT algorithm without additional smoothing. The chart highlights the values of the statistical parameters measured for the enhanced images. The blue bars in the chart depict the PSNR value,

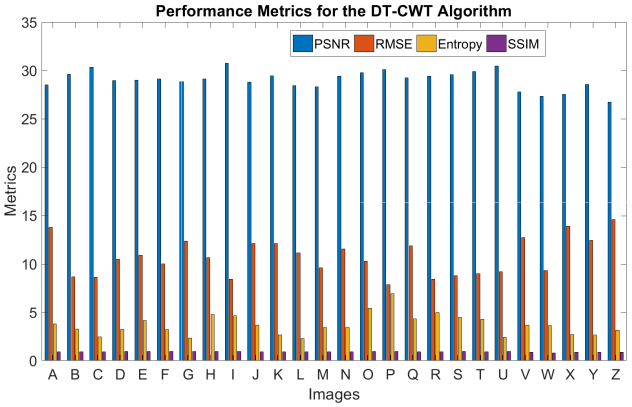

FIGURE 8. DTCWT-induced changes in image contrast: A statistical view.

which averages 29.22 dB. The orange bars in the chart depict the average RMSE value, measuring 10.61, indicating relatively higher errors. The yellow-colored bars in the chart represent the average Entropy, calculated at 3.69, which indicates sub-optimality. Finally, violet-colored bars in the chart depict the average SSIM value of 0.93, suggesting a relatively lower structural similarity. Finally, the chart reveals that applying the DTCWT algorithm alone leads to suboptimal image quality. The proposed DT-CWT and EPS algorithm images are decomposed into different subbands and interpolated, after which subbands are reconstructed to achieve the enhanced image. The input image is first performed decomposition using the wavelet transformation method. The wavelet transformation will be performed with respect to discrete and continuous wavelet transforms; the level of decomposition is also specified during the process. In the DWT, the source function cast off the 'symlet' mama wavelet. After the application of DWT into the image, the image is decomposed into 2 parts: the estimated and meticulous quantities. The approximation quantities are taken into consideration. A similar procedure is applied to CWT. The obtained decomposed approximation quantities are sent to the interpolation block for further processing.

Figure 9 shows the overall graph representing the results of resolution enhancement for the set of 26 images. The enhancement was achieved using DT-CWT in conjunction with an edge preservation smoothing algorithm called EPS. EPS employs a Gaussian low-pass filter to preserve essential image features such as homogeneous regions, edges, discontinuities, and textures. The graph highlights the values of the statistical parameters measured for the enhanced images. The blue-colored bars in the chart represent the PSNR value, which averages 30.35 dB. The orange bars in the graph depict the average RMSE value, measuring 9.38, indicating relatively lower errors. The yellow-colored bars in the chart represent the average Entropy, calculated at 1.96. Finally, the violet-colored bars in the graph show the average SSIM value of 0.97, suggesting a relatively improved structural similarity. Finally, the chart reveals that applying the DT-CWT in conjunction with an edge preservation smoothing algorithm improves image quality.

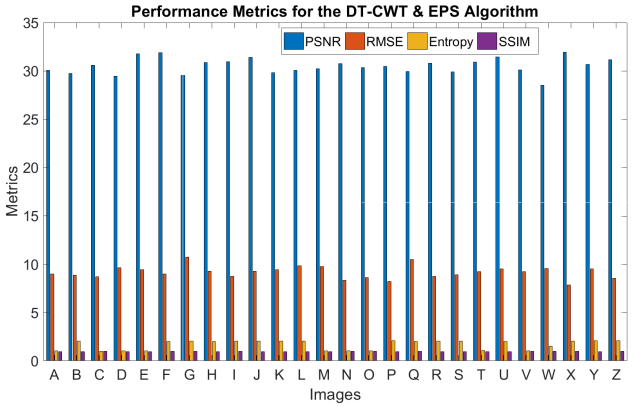

FIGURE 9. DTCWT & EPS-induced changes in image contrast: A statistical view.

Figure 10 illustrates a dedicated Graphical User Interface (GUI) meticulously crafted to facilitate the execution of the DWT operation, utilizing Haar wavelets, on the designated query image. This interface is ingeniously designed to empower users in the extraction of pivotal image coefficients, achieved by employing the DWT process. The rationale behind adopting Haar wavelets lies in their inherent efficiency, which lends itself exceptionally well to the representation and comprehensive analysis of image characteristics. The DWT serves as a mathematical mechanism, serving the purpose of decomposing an input image into distinct frequency constituents. This dissection brings to light the image's intricate structural nuances, discernible across varying scales.

Figure 10 shows the resulting LL (Low-Low), LH (Low-High), HL (High-Low), and HH (High-High) sub-band coefficients from the DWT operation. LL: Approximate image representing low-frequency components. LH: Extracts horizontal features from the original image. HL: Provides vertical features. HH: Captures diagonal features. The focus during query processing is on the LL sub-band of the query image. Flat-perpendicular prognoses are applied to aid the process, with pre-calculated even and perpendicular silhouettes for all images in the preparation database. The extraction and utilization of these sub-band coefficients, along with the flat-perpendicular prognoses, play a critical role in enhancing the efficiency and accuracy of the VBIR system, thereby improving the retrieval and reclamation of similar images from the database. These scientifically informed processes contribute to the advancement of medical image analysis and retrieval techniques for better patient care and clinical decision-making.

Figure 11(a) and Figure 11(b) demonstrate the processes of flat summation and perpendicular summation on the query image matrix. These summations involve using global variables to facilitate computations. The study aims to derive flat and perpendicular projections using the lower coefficients. The flat projection obtained through flat summation is crucial for computing edge descriptors. Conversely, the perpendicular projection achieved through perpendicular summation

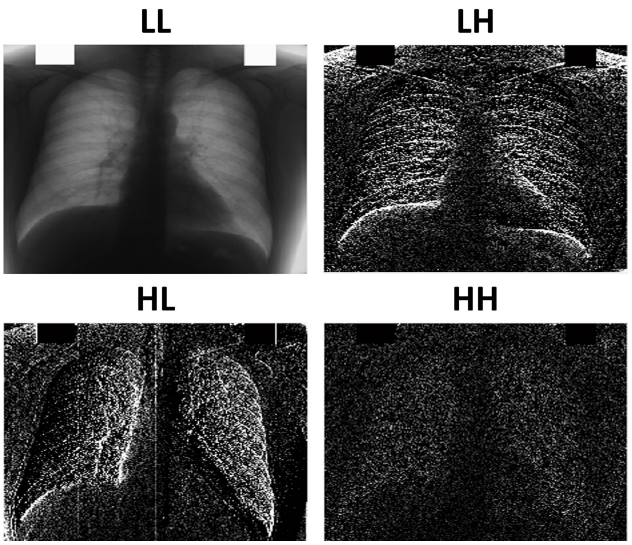

FIGURE 10. Quantifying wavelet transformation breakdown: Analyzing LL, LH, HL, and HH Components.

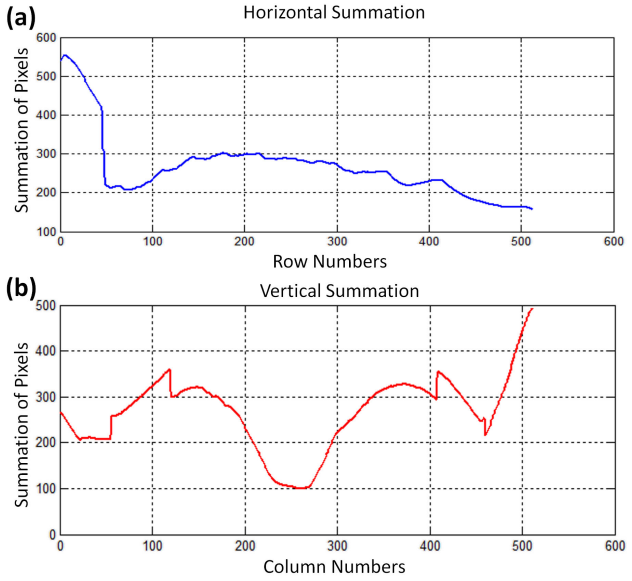

FIGURE 11. (a) Quantifying row intensity: The flat summation analysis, and (b)Quantifying Column Intensity: perpendicular summation analysis.

enables the system to compare and evaluate the similarity between different images based on their perpendicular edge characteristics. By incorporating both flat and perpendicular projections derived from lower coefficients, the system gains valuable insights into the image's edge properties and directional features. This approach enhances the system's ability to recognize and analyze image content based on these important visual cues.

Figure 12(a) and Figure 12(b) demonstrate the horizontal projection and perpendicular projection obtained by calculating the histogram of the column-wise sum vectors and row sum vectors of the image. By applying the histogram function to the flat ($FP(i) = H(FSV, i)$) and perpendicular summation vector ($PP(i) = H(PSV, i)$), we acquire the flat and perpendicular histogram projection. This results

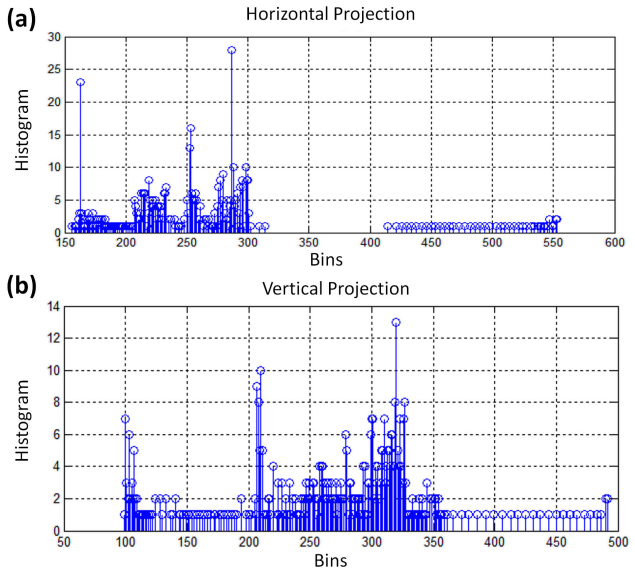

FIGURE 12. (a) Prognosticating pixel behavior: The flat prognose perspective, and (b) Prognosticating pixel behavior: The perpendicular prognose perspective.

in a dense distribution of projection values in the 50-300 bins range for the flat summation values. The perpendicular projection captures edge features present in the perpendicular direction of the image. It visually represents the distribution of these features along the perpendicular axis, enabling further identification of unique patterns related to orientation. The histogram projection of perpendicular summation values shows a dense distribution of projection values in the 100-350 bins range. The matching score (MS_p) calculation using prognose between two images I and J based on their prognose projections (FP_I, PP_I, FP_J), *and* PP_J is computed using Equation 9

$$MS_p(I,J) = \frac{2 \cdot (FP_I \cdot FP_J + PP_I \cdot PP_J)}{FP_I^2 + FP_J^2 + PP_I^2 + PP_J^2} \tag{9}$$

By incorporating both flat and perpendicular projections derived from the lower coefficients, the system gains valuable insights into the images' edge properties and directional features. These scientifically informed techniques contribute to enhancing the efficiency and accuracy of image analysis and retrieval in the context of VBIR systems, thereby advancing medical imaging research and clinical decision-making.

In Figure 13, the retrieved image from the proposed framework is displayed, revealing a poor match in the database. The Bhattacharya Coefficient for this retrieved image is significantly low, i.e. 220, indicating a low level of similarity with the query image. This discrepancy can be attributed to several factors, including variability in image characteristics, insufficient feature representation, and the small size of the database. The matching score between two images I and J based on their Bhattacharya Coefficient values (BC_I and BC_J) is calculated as Equation 10

$$BS(I,J) = \frac{2 \cdot BC_I \cdot BC_J}{BC_I + BC_J}. \tag{10}$$

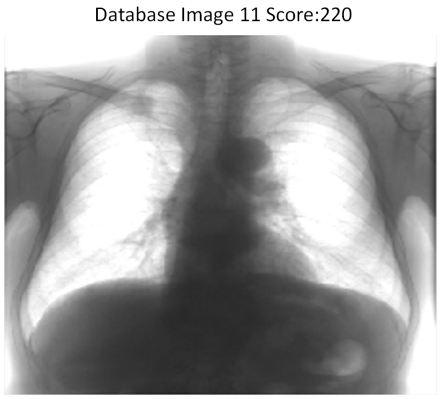

FIGURE 13. Uncommon visual traits: Insights from a Low Bhattacharya Score.

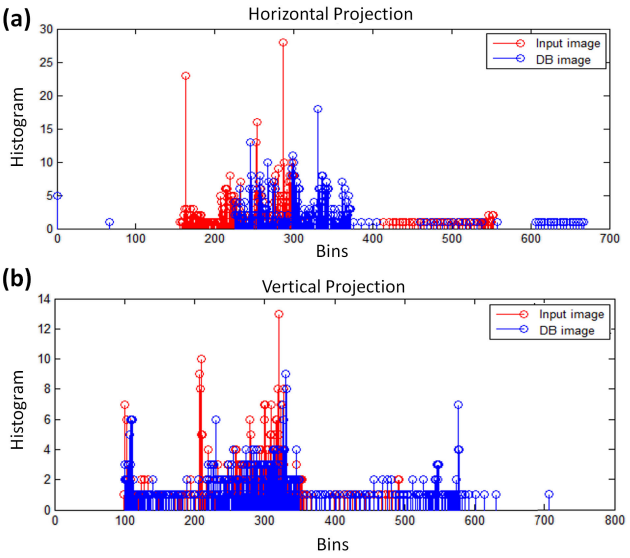

FIGURE 14. (a)The prognosticator's perspective: Significance of flat Prognose convergence, and (b)The prognosticator's perspective: significance of perpendicular prognose convergence.

Figure 14(a) illustrates the flat prognose projection obtained by computing the column-wise sum vectors of the image. The resulting flat prognose projection shows a low matching score of 220, allowing for the analysis and visualization of feature distribution along the flat axis. The red bars in the graph represent the projection of the query image, while the blue bars represent the projection of the database values. Images in the database generate larger coefficient values, indicating a lower degree of resemblance between them. The prognose function keeps a count of the measured features, allowing for the analysis and visualization of their distribution along the flat axis. This projection captures edge features present in the perpendicular direction of the image, providing a visual representation of their distribution along the perpendicular axis, enabling in-depth analysis and examination of their characteristics.

Figure 14(b) shows the perpendicular prognose projection obtained from the row sum vectors of the image. Applying a prognose function to the perpendicular summation vector yields a projection with a low matching score of 220. The

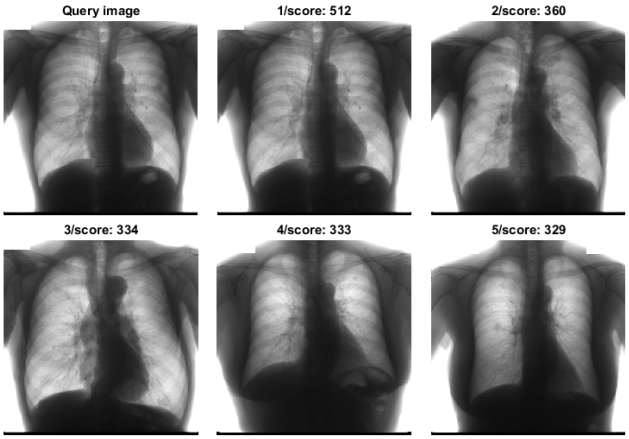

FIGURE 15. Visual excellence: The elite group of high B-Score retrievals.

red bars represent the projection of the query image, while the blue bars represent the projection of the database values, indicating a lower degree of resemblance between them.

Despite the poor matching score in this specific case, the analysis provided by these projections is valuable in identifying potential areas of improvement for the image retrieval process. It offers a deeper understanding of the similarities and differences between the query image and the database images, providing guidance for refining the matching algorithm and enhancing the accuracy of the image retrieval system in the future.

Figure 15 presents the top 5 highest matching results from the database based on the Bhattacharya Coefficient (B score). These high coefficient values indicate significant similarity between retrieved and query images. A higher coefficient value suggests a stronger resemblance, reflecting close matches in their characteristics. The coefficient values for the top 5 matches are 512, 360, 334, 333, and 329, respectively. Sorting the coefficient vector in descending order enables efficient retrieval of images that closely match the query image's characteristics. This process ensures the identification of images in the database that are most similar to the query image, facilitating effective image retrieval based on their similarities.

Higher coefficient values indicate a stronger resemblance between the query and database images in this method. To identify the images in the database that are most similar to the query image, the coefficient vector is sorted in descending order, and the images corresponding to the larger coefficient values are selected. This approach allows for an efficient retrieval of images that closely match the characteristics of the query image, facilitating the image reclamation process with improved accuracy and effectiveness.

Figure 16 presents the plot of the B score for a collection of images in the database. The results reveal that around 11 images have a B score above 300, indicating a significant relationship with the query image. Among these, two images have a B score close to 350, signifying a strong resemblance or similarity to the query image. However, the majority of the images show a sub-optimal resemblance to the query image,

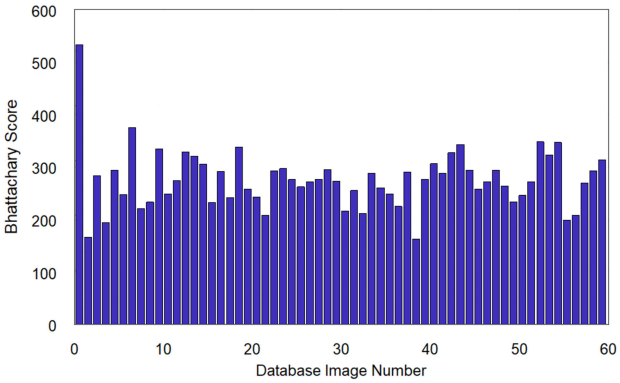

FIGURE 16. The bhattacharya spectrum: A visual insight into image distinctiveness.

TABLE 1. Assessment of retrieval accuracy: proposed method vs. prior work.

Method	Retrieval Accuracy (%)
Kumar and Mohan [49]	86.80
Tarjoman et al. [50]	90.09
Praveena et al. [51]	98.88
Battur and Jagadisha [52]	97.00
Proposed VBIR method	**97.54**

as they have lower B scores. This suggests that they are less similar to the query image compared to the top matching results. Overall, the B score plot helps to assess the similarity between the query image and the images in the database, with higher B scores indicating stronger matches and lower scores indicating weaker matches. The two images with scores close to 350 are likely to be the most similar to the query image, while the rest of the images may have varying degrees of dissimilarity.

The rigorous performance evaluation of the proposed VBIR technique includes a thorough comparison with existing methodologies, which utilize the database, as meticulously summarized in Table 1. The findings from this comprehensive analysis unequivocally affirm the proposition's significance, making a compelling case for its status as a state-of-the-art solution in the dynamic domain of image retrieval. The assessment of retrieval accuracy is a focal point of this evaluation, involving a careful juxtaposition of the proposed VBIR technique's performance against several noteworthy existing methods: Kumar and Mohan [49] Attained a retrieval accuracy of 86.80%, Tarjoman et al. [50]: Achieved a retrieval accuracy of 90.09%, Praveena et al. [51]: Demonstrated a retrieval accuracy of 98.88%, Battur and Jagadisha [52]: Registered a retrieval accuracy of 97.00%, Proposed VBIR method: Showcased a remarkable retrieval accuracy of 97.54%.

These meticulous comparisons undeniably establish the proposed VBIR technique as a leader in the field, consistently rivaling or surpassing existing state-of-the-art methods. Its exceptional accuracy rate of 97.54% underscores its contemporary relevance and capability to meet the evolving demands of image retrieval.

The enhanced VBIR system with good Bhattacharya Coefficients (B scores) demonstrates improved accuracy

and effectiveness in the image reclamation process. The combination of Bhattacharyya coefficient, intersection of bins, alpha calculation, and DWT ensures the accuracy and effectiveness of the reclamation process, making it a valuable tool for medical image analysis and diagnosis. The incorporation of these techniques provides researchers and practitioners with a powerful and reliable system for medical image reclamation with potential applications in various research domains.

V. CONCLUSION

This research introduces a pioneering approach in the domain of medical image processing, specifically tailored to enhance the retrieval and resolution of chest X-ray images through a VBIR technique. This innovative methodology seamlessly integrates the DT-CWT with Edge Preservation Smoothing (EPS) filtering, resulting in a range of significant advantages. On the positive side, this approach notably enhances image quality. The utilization of DT-CWT, renowned for its shift invariance and directional selectivity, plays a pivotal role in elevating image quality. Further refinement is achieved by combining DT-CWT with EPS filtering, which yields the highest PSNR and the lowest RMSE and Entropy values. The result is a collection of images that are clearer and possess heightened diagnostic value.

Additionally, this approach streamlines the image retrieval process, making it more accurate and efficient. By incorporating Bhattacharya Coefficients and DT-CWT, the retrieval of relevant medical images becomes more precise, ultimately enhancing the capabilities of medical professionals in their diagnostic tasks. Moreover, our research maintains a strong commitment to objective evaluation. We employ a comprehensive set of quantitative metrics, including PSNR, SSIM, RMSE, and Entropy, to rigorously assess image quality and retrieval accuracy. This meticulous evaluation methodology enhances the credibility of our findings.

Furthermore, practical applicability is demonstrated through extensive experimentation on a dataset containing 60 chest X-ray samples. The experimental results demonstrated the effectiveness of our approach, achieving impressive scores of PSNR 31, SSIM 0.99, RMSE 8.25, and entropy 1.03. Moreover, the experimental evaluations proved the algorithm's efficiency and effectiveness by significantly enhancing the retrieval score of the top 5 matching images from 320 to 512. The results emphasize the real-world potential of our research, with high PSNR scores, SSIM values approaching unity, low RMSE values, and minimal entropy values. Nevertheless, it is essential to acknowledge that integrating advanced techniques like DT-CWT and EPS filtering may introduce a level of complexity to the image processing workflow, potentially necessitating specialized knowledge and computational resources for implementation. Overall, this research significantly advances the field of medical image processing, offering a comprehensive solution to the challenges of chest X-ray image enhancement and retrieval. Its reliance on quantitative evaluation metrics and robust experimental results establishes its credibility and potential to enhance the diagnostic capabilities of medical professionals, ultimately leading to improved patient care and outcomes in chest-related medical conditions.

APPENDIX

The provided algorithm implements a wavelet-based decomposition technique for image processing. It applies the DWT to decompose the input image into its approximation and detail coefficients at different levels of resolution. The algorithm also includes interpolation methods like nearest neighbor, bilinear filtering, and bi-cubic interpolation for image resizing and enhancing image quality. The DWT enables efficient dimensionality reduction, feature extraction, and multi-resolution representation of images, while the interpolation methods aid in image reconstruction. These techniques are commonly used in various image processing applications to improve image quality, and facilitate other image-related tasks.

A. ALGORITHM FOR WAVELET-BASED DECOMPOSITION

The wavelet-based decomposition algorithm aims to transform an input image I into its multi-resolution representation using wavelet transforms. The process involves iteratively obtaining approximation coefficients (low-frequency sub-bands) and detail coefficients (high-frequency sub-bands) for different levels of decomposition. The pseudocode for the algorithm is as follows:

Algorithm 2 Wavelet-Based Decomposition Algorithm

```
Load image I Data: Initialize level x, x = x/2
Result: Multi-resolution representation of I
for m = 1 to 2 do
    for n = 1 to 2 do
        [low1mn] = get approximation coefficients;
        for j = 2 to J do
            [lowjmn] = get detail coefficients;
        end
    end
end
```

B. ALGORITHM FOR NEAREST NEIGHBOR INTERPOLATION

The nearest neighbor interpolation method is used to resize an image by computing the pixel values of the new image based on the values of the nearest neighboring pixels from the original image. The pseudocode for the algorithm is as follows:

C. ALGORITHM FOR BILINEAR FILTERING

The bilinear filtering method is used for image interpolation, providing a smoother, more visually appealing resized image. The algorithm computes the average of neighboring pixels to

Algorithm 3 Nearest Neighbor Interpolation Algorithm

Load image I **Data:** Initialize preprocess, order, Avg1, Avg2, out
$preprocess$ = convert image from RGB to grayscale;
$order$ = compute order of the image;
compute interpolation weights and indices for the image;
$Avg1$ = compute the average of the neighboring pixels along rows;
$Avg2$ = compute the average of the neighboring pixels along columns;
out = nearest neighbor interpolated image;

Algorithm 4 Bilinear Filtering Algorithm

Load image I **Data:** Initialize preprocess, order, Avg, out
$preprocess$ = convert image from RGB to grayscale;
$order$ = compute order of the image;
compute interpolation weights and indices for the image;
Avg = compute average of the neighboring pixels;
out = bilinear interpolated image;

estimate the pixel values of the new image. The pseudocode for the algorithm is as follows:

D. ALGORITHM FOR BICUBIC INTERPOLATION

The bicubic interpolation method is a higher-order interpolation technique used to enhance the image quality during resizing. It computes the pixel values based on a cubic polynomial using neighboring pixel intensities. The pseudocode for the algorithm is as follows:

Algorithm 5 Bicubic Interpolation Algorithm

Load image I **Data:** Initialize preprocess, order, Avg1, Avg2, abs, abs2, abs3, f, out
$preprocess$ = convert image from RGB to grayscale;
$order$ = compute order of the image;
compute interpolation weights and indices for the image;
$Avg1$ = compute average of the neighboring pixels along rows;
$Avg2$ = compute average of the neighboring pixels along columns;
abs = compute absolute value for the image;
$abs2 = abs^2$;
$abs3 = abs^3$;
$f = (1.5 * abs^3 - 2.5 * abs^2 + 1) .* (abs <= 1) + (-0.5 * abs^3 + 2.5 * abs^2 - 4 * abs + 2) .* ((1 < abs)\&(abs <= 2))$;
out = nearest neighbor interpolated image;

E. ALGORITHM FOR BILATERAL FILTERING (DT-CWT AND EPS)

The bilateral filtering algorithm combines DT-CWT and EPS techniques for image filtering. The process involves computing the mean and standard deviations of the image and using them to determine the window size. Gaussian distribution weights are calculated to extract the local region, and Gaussian intensity weights are computed. Finally, the frequency response is obtained using the weighted values. The pseudocode for the algorithm is as follows:

Algorithm 6 Bilateral Filtering Algorithm (DT-CWT and EPS)

Load image I **Data:** Compute mean and standard deviations
Data: Initialize window size
Data: Compute Gaussian distribution weights
for *each pixel* (i, j) *in the image* **do**
  Extract local region, a;
  Compute Gaussian intensity weights;
  Compute frequency response;
  $F = H \cdot G((iMin : iMax) - i + w + 1, (jMin : jMax) - j + w + 1)$;
  $B = \frac{\sum F(\text{all rows of image } F) \cdot I(\text{all rows of image } I)}{\sum F(\text{all rows of image } F)}$;
end

The wavelet-based decomposition algorithm utilizes the DWT to decompose the input image into four subbands: LL (low-frequency approximation), LH (horizontal details), HL (vertical details), and HH (diagonal details). This multi-resolution representation allows for efficient feature extraction and enhanced image processing capabilities.

The nearest neighbor interpolation method computes the new pixel values by selecting the intensity of the nearest neighboring pixels from the original image. While computationally simple, it may lead to blocky artifacts and loss of fine details.

The bilinear filtering method provides a smoother interpolation by computing the weighted average of neighboring pixel intensities. It produces better results compared to nearest neighbor interpolation, retaining more image details.

The bi-cubic interpolation method offers even higher quality image resizing by using a cubic polynomial to estimate pixel values based on neighboring pixel intensities. This technique results in a visually superior image with reduced distortion.

Finally, the bilateral filtering algorithm combines DT-CWT and EPS techniques to achieve edge-preserving image filtering. By computing Gaussian distribution and intensity weights, it effectively removes noise while preserving important image features.

REFERENCES

[1] J. Li, J. Chen, Y. Tang, C. Wang, B. A. Landman, and S. K. Zhou, "Transforming medical imaging with transformers? A comparative review of key properties, current progresses, and future perspectives," *Med. Image Anal.*, vol. 85, Apr. 2023, Art. no. 102762.

[2] N.-N. Zhong, H.-Q. Wang, X.-Y. Huang, Z.-Z. Li, L.-M. Cao, F.-Y. Huo, B. Liu, and L.-L. Bu, "Enhancing head and neck tumor management with artificial intelligence: Integration and perspectives," in *Seminars in Cancer Biology*. Amsterdam, The Netherlands: Elsevier, 2023.

[3] X. Zhang, C. Wu, Y. Zhang, W. Xie, and Y. Wang, "Knowledge-enhanced visual-language pre-training on chest radiology images," *Nature Commun.*, vol. 14, no. 1, p. 4542, Jul. 2023.

[4] P. Müller, G. Kaissis, C. Zou, and D. Rueckert, "Radiological reports improve pre-training for localized imaging tasks on chest X-rays," in *Proc. Int. Conf. Med. Image Comput. Comput.-Assist. Intervent.* Springer, 2022, pp. 647–657.

[5] B. Ferreira, J. Rodrigues, J. Leitão, and H. Domingos, "Privacy-preserving content-based image retrieval in the cloud," in *Proc. IEEE 34th Symp. Reliable Distrib. Syst. (SRDS)*, Sep. 2015, pp. 11–20.

[6] L. Xing, M. L. Giger, and J. K. Min, *Artificial Intelligence in Medicine: Technical Basis and Clinical Applications*. New York, NY, USA: Academic, 2020.

[7] A. A. Mukhlif, B. Al-Khateeb, and M. A. Mohammed, "An extensive review of state-of-the-art transfer learning techniques used in medical imaging: Open issues and challenges," *J. Intell. Syst.*, vol. 31, no. 1, pp. 1085–1111, Sep. 2022.

[8] N. Ismail, A. Venault, J.-P. Mikkola, D. Bouyer, E. Drioli, and N. T. H. Kiadeh, "Investigating the potential of membranes formed by the vapor induced phase separation process," *J. Membrane Sci.*, vol. 597, Mar. 2020, Art. no. 117601.

[9] Z. Wang, Y. Lv, R. Wu, and Y. Zhang, "Review of GrabCut in image processing," *Mathematics*, vol. 11, no. 8, p. 1965, Apr. 2023.

[10] B. B. Sinha and R. Dhanalakshmi, "Evolution of recommender system over the time," *Soft Comput.*, vol. 23, no. 23, pp. 12169–12188, Dec. 2019.

[11] M. H. Memon, J.-P. Li, I. Memon, and Q. A. Arain, "GEO matching regions: Multiple regions of interests using content based image retrieval based on relative locations," *Multimedia Tools Appl.*, vol. 76, no. 14, pp. 15377–15411, Jul. 2017.

[12] N. B. Thylstrup, D. Agostinho, A. Ring, C. D'Ignazio, and K. Veel, *Uncertain Archives: Critical Keywords for Big Data*. Cambridge, MA, USA: MIT Press, 2021.

[13] M. Costa, E. Kangasjarvi, and A. Charise, "Beyond empathy: A qualitative exploration of arts and humanities in pre-professional (baccalaureate) health education," *Adv. Health Sci. Educ.*, vol. 25, no. 5, pp. 1203–1226, Dec. 2020.

[14] J. Yue, Z. Li, L. Liu, and Z. Fu, "Content-based image retrieval using color and texture fused features," *Math. Comput. Model.*, vol. 54, nos. 3–4, pp. 1121–1127, Aug. 2011.

[15] Q. Cheng, S. Zhang, X. Chen, H. Cui, Y. Xu, S. Xia, K. Xia, T. Zhou, and X. Zhou, "Inversion of reclaimed soil water content based on a combination of multi-attributes of ground penetrating radar signals," *J. Appl. Geophys.*, vol. 213, Jun. 2023, Art. no. 105019.

[16] E. Yildizer, A. M. Balci, M. Hassan, and R. Alhajj, "Efficient content-based image retrieval using multiple support vector machines ensemble," *Expert Syst. Appl.*, vol. 39, no. 3, pp. 2385–2396, Feb. 2012.

[17] M. S. Kumar, J. Rajeshwari, and N. Rajasekhar, "Exploration on content-based image retrieval methods," in *Pervasive Computing and Social Networking*. Springer, 2022, pp. 51–62.

[18] M. Sharma and A. Batra, "Analysis of distance measures in content based image retrieval," *Global J. Comput. Sci. Technol.*, vol. 14, no. 2, p. 7, 2014.

[19] M. Guo, Z. Yu, Y. Xu, Y. Huang, and C. Li, "ME-Net: A deep convolutional neural network for extracting mangrove using Sentinel-2A data," *Remote Sens.*, vol. 13, no. 7, p. 1292, Mar. 2021.

[20] H. Liu, X. Huang, R. Tang, Y. Min, Q. Xu, Z. Hu, and P. Shi, "Simultaneous peeling of precious metals in cathode and anode of spent ternary batteries using electrolysis," *Separat. Purification Technol.*, vol. 313, May 2023, Art. no. 123478.

[21] N. Varish, J. Pradhan, and A. K. Pal, "Image retrieval based on non-uniform bins of color histogram and dual tree complex wavelet transform," *Multimedia Tools Appl.*, vol. 76, no. 14, pp. 15885–15921, Jul. 2017.

[22] A. S. M. Priyadharson, C. Thilipkumar, and L. M. K. Reddy, "Sentinel-2 satellite image enhancement and compression based on DWT and vector quantization," in *Artificial Intelligence and Machine Learning in Satellite Data Processing and Services*. Springer, 2023, pp. 1–7.

[23] J. P. Gawande, A. D. Rahulkar, and R. S. Holambe, "Efficient rationalization of triplet halfband filter banks and its application to image compression," *IEEE Trans. Circuits Syst. Video Technol.*, vol. 30, no. 11, pp. 4020–4033, Nov. 2020.

[24] B. J. McKee, S. M. Regis, A. B. McKee, S. Flacke, and C. Wald, "Performance of ACR lung-RADS in a clinical CT lung screening program," *J. Amer. College Radiol.*, vol. 13, no. 2, pp. R25–R29, Feb. 2016.

[25] S. J. van Riel, C. I. Sánchez, A. A. Bankier, D. P. Naidich, J. Verschakelen, E. T. Scholten, P. A. de Jong, C. Jacobs, E. van Rikxoort, L. Peters-Bax, M. Snoeren, M. Prokop, B. van Ginneken, and C. Schaefer-Prokop, "Observer variability for classification of pulmonary nodules on low-dose CT images and its effect on nodule management," *Radiology*, vol. 277, no. 3, pp. 863–871, Dec. 2015.

[26] M. Cedillo-Hernandez, F. J. Garcia-Ugalde, A. Cedillo-Hernandez, M. Nakano-Miyatake, and H. Perez-Meana, "Content based video retrival system for Mexican culture heritage based on object matching and local–global descriptors," in *Proc. Int. Conf. Mechatronics, Electron. Automot. Eng.*, Nov. 2014, pp. 38–43.

[27] K. Kunze, H. Kawaichi, K. Yoshimura, and K. Kise, "The wordometer—Estimating the number of words read using document image retrieval and mobile eye tracking," in *Proc. 12th Int. Conf. Document Anal. Recognit.*, Aug. 2013, pp. 25–29.

[28] Poonam and S. M. Arora, "A DWT-SVD based robust digital watermarking for digital images," *Proc. Comput. Sci.*, vol. 132, pp. 1441–1448, Jan. 2018.

[29] Y. Li, D. Zeng, L. Gu, Q. Chen, S. Guo, A. Zomaya, and M. Guo, "Efficient and secure deep learning inference in trusted processor enabled edge clouds," *IEEE Trans. Parallel Distrib. Syst.*, vol. 33, no. 12, pp. 4311–4325, Dec. 2022.

[30] N. Sharma, V. Kumar, and S. K. Singla, "Single image defogging using deep learning techniques: Past, present and future," *Arch. Comput. Methods Eng.*, vol. 28, no. 7, pp. 4449–4469, Dec. 2021.

[31] D. Wen, X. Huang, F. Bovolo, J. Li, X. Ke, A. Zhang, and J. A. Benediktsson, "Change detection from very-high-spatial-resolution optical remote sensing images: Methods, applications, and future directions," *IEEE Geosci. Remote Sens. Mag.*, vol. 9, no. 4, pp. 68–101, Dec. 2021.

[32] F. Ahmad, A. Farooq, and M. U. Ghani, "Deep ensemble model for classification of novel coronavirus in chest X-ray images," *Comput. Intell. Neurosci.*, vol. 2021, pp. 1–17, Jan. 2021.

[33] P. K. B. Rangaiah, J. Ebrahimizadeh, A. H. Nagaraju, I. El-Ali, M. Kouki, B. Mandal, F. Huss, M. D. Perez, and R. Augustine, "Clustering of dielectric and colour profiles of an ex-vivo burnt human skin sample," in *Proc. 14th Eur. Conf. Antennas Propag. (EuCAP)*, Mar. 2020, pp. 1–5.

[34] P. K. B. Rangaiah, M. Kouki, Y. Dhouibi, F. Huss, B. Mandal, B. Augustine, M. D. Perez, and R. Augustine, "Dielectric characterization and statistical analysis of ex-vivo burnt human skin samples for microwave sensor development," *IEEE Access*, vol. 11, pp. 4359–4372, 2023.

[35] M. Melek, A. Khattab, and M. F. Abu-Elyazeed, "Fast matching pursuit for sparse representation-based face recognition," *IET Image Process.*, vol. 12, no. 10, pp. 1807–1814, Oct. 2018.

[36] Z. Zheng, Y. Wan, Y. Zhang, K. Yang, R. Xiao, C. Lin, Q. Wu, and D. Peng, "EMS-CDNet: An efficient multi-scale-fusion change detection network for very high-resolution remote sensing images," *Int. J. Remote Sens.*, vol. 43, no. 14, pp. 5252–5279, Jul. 2022.

[37] M. Kiruban, R. Jayamani, and P. Ramu, "Removal of salt and pepper noise from SAR images using optimized APCNN in shearlet transform domain," *Arabian J. Geosci.*, vol. 14, no. 6, pp. 1–10, Mar. 2021.

[38] X. Liu, C. Vlachou, M. Yang, F. Qian, L. Zhou, C. Wang, L. Zhu, K.-H. Kim, G. Parmer, Q. Chen, and K.-H. Kim, "Firefly: Untethered multi-user VR for commodity mobile devices," in *Proc. USENIX Annu. Tech. Conf. (USENIX ATC)*, 2020, pp. 943–957.

[39] M. R. Sankar, P. Srinivas, V. Praveena, D. Bhavani, M. S. U. Suseela, Y. Srinivas, and C. V. Rao, "Performance evaluation of multiwavelet transform for single image dehazing," in *Proc. Int. Conf. Cogn. Comput. Cyber Phys. Syst.* Springer, 2022, pp. 125–133.

[40] P. M. Kamble, D. D. Ruikar, K. V. Houde, and R. S. Hegadi, "Adaptive threshold-based database preparation method for handwritten image classification," in *Proc. Int. Conf. Recent Trends Image Process. Pattern Recognit.* Springer, 2021, pp. 280–288.

[41] S. Liu, J. Feng, and Z. Tian, "Variational low-rank matrix factorization with multi-patch collaborative learning for hyperspectral imagery mixed denoising," *Remote Sens.*, vol. 13, no. 6, p. 1101, Mar. 2021.
[42] P. Prasenan and C. D. Suriyakala, "A study of underwater image pre-processing and techniques," in *Computational Vision and Bio-Inspired Computing*. Springer, 2022, pp. 313–333.
[43] D. Javaheri, S. Gorgin, J.-A. Lee, and M. Masdari, "Fuzzy logic-based DDoS attacks and network traffic anomaly detection methods: Classification, overview, and future perspectives," *Inf. Sci.*, vol. 626, pp. 315–338, May 2023.
[44] P. S. Thakur, P. Khanna, T. Sheorey, and A. Ojha, "Trends in vision-based machine learning techniques for plant disease identification: A systematic review," *Expert Syst. Appl.*, vol. 208, Dec. 2022, Art. no. 118117.
[45] A. Jaszcz, D. Połap, and R. Damaševičius, "Lung X-ray image segmentation using heuristic red fox optimization algorithm," *Sci. Program.*, vol. 2022, pp. 1–8, Jul. 2022.
[46] D. Połap and M. Woźniak, "Red fox optimization algorithm," *Expert Syst. Appl.*, vol. 166, Mar. 2021, Art. no. 114107.
[47] T. B. Mary I, P. M. Bruntha, M. A. P. Manimekalai, K. M. Sagayam, and H. Dang, "Investigation of an efficient integrated semantic interactive algorithm for image retrieval," *Pattern Recognit. Image Anal.*, vol. 31, no. 4, pp. 709–721, Oct. 2021.
[48] S. Tyagi and D. Yadav, "A detailed analysis of image and video forgery detection techniques," *Vis. Comput.*, vol. 39, no. 3, pp. 813–833, Mar. 2023.
[49] G. V. S. Kumar and P. G. K. Mohan, "Improved content based image retrieval process based on deep convolutional neural network and salp swarm algorithm," *Int. J. Image Graph.*, vol. 22, no. 5, Oct. 2022, Art. no. 2250047.
[50] M. Tarjoman, E. Fatemizadeh, and K. Badie, "An implementation of a CBIR system based on SVM learning scheme," *J. Med. Eng. Technol.*, vol. 37, no. 1, pp. 43–47, Jan. 2013.
[51] H. D. Praveena, N. S. Guptha, A. Kazemzadeh, B. D. Parameshachari, and K. L. Hemalatha, "Effective CBMIR system using hybrid features-based independent condensed nearest neighbor model," *J. Healthcare Eng.*, vol. 2022, pp. 1–9, Mar. 2022.
[52] R. Battur and N. Jagadisha, "A performance aware content based image retrieval (CBIR) technique," *Int. J. Inf. Technol. Secur.*, vol. 14, no. 2, pp. 87–98, 2022.

B. P. PRADEEP KUMAR received the B.E. degree in electronics and communication from SJMIT, Chitradurga, the M.Tech. degree in DCE from AIT, Bengaluru, and the Ph.D. degree in electronics engineering from Jain University. He is currently a distinguished electronics and communication engineering researcher. He is also an Associate Professor with the Department of Electronics and Communication Engineering, HKBKCE, Bengaluru. He actively participates in various academic governing bodies, such as IQAC, NBA, NAAC auditing, BOS, and BOE, contributing significantly to the advancement of academic standards. He has a remarkable track record, having filed 15 patents and served as an advisory committee member and the session chair for international conferences organized by IEEE/Springer. In addition to these achievements, he has also undertaken roles like a PG coordinator and has an impressive publication record, with more than 56 research articles and ten authored books to his credit.

PRAMOD K. B. RANGAIAH (Member, IEEE) received the B.E. degree in electronics and communication from the Dr. Ambedkar Institute of Technology, Bengaluru, and the M.Tech. degree in R. F. communication and the Ph.D. degree in electronics engineering from Jain University, Bengaluru. He is currently a distinguished researcher in microwaves in medical engineering. He holds the position of a Researcher with Ångström Laboratoriet, Uppsala Universitet, Sweden. He is also a recognized expert. He has industry experience as an R. F. Design Trainee with Icon Design and Automation Pvt Ltd., and has conducted research as a Visiting Scholar with the University of Concordia, Montreal, QC, Canada. He actively contributes to scholarly publishing as an Associate Editor of *IJBDM* (Inderscience Publishers) and through roles on the editorial boards of Frontiers and *IJAAS*. He is also a peer-reviewer for esteemed international journals, including IEEE Access, MDPI, Inderscience Publishers, *ASTESJ*, and *IJARIIE*. His research interests include microwaves in medical engineering, covering various aspects, such as R. F. passive device design, board-level tuning, low-noise amplifiers, power amplifiers, circuit linearization, high-efficiency design techniques, and circuit instability strategies. He is dedicated to advancing the field and is widely respected for his contributions and expertise.

ROBIN AUGUSTINE (Member, IEEE) received the degree in electronics science from Mahatma Gandhi University, India, in 2003, the master's degree in electronics with robotics specialization from the Cochin University of Science and Technology, India, in 2005, and the Ph.D. degree in electronics and optic systems from the Univerisité Paris-Est Marne-La-Vallée, France, in July 2009. He was a Post-Doctoral Researcher at the University of Rennes 1, Brittany, France, from 2009 to 2011. He joined Uppsala University as a Senior Researcher in 2011. He became an Associate Professor with Uppsala University in February 2016. He is currently a Senior University Lecturer in medical engineering and a Docent in microwave technology. He is also the Head of the Microwaves in Medical Engineering Group (MMG), and the Founder, the Chairperson, and the CTO of Probingon AB, Swedish Medtech Company. He was a part of Vinnova Project on skin cancer diagnostic tool based on micromachined interface for high-resolution THz spectroscopy (MTSSC). He is a Co-PI of the EU Project SINTEC, SSF framework grant LifeSec, Vinnova grant connect my body, in 2018, and the SSF framework grant Zero-IoT 2020, the Research Lead of the Eurostars Project SenseBurn 2018, and the Project Leader of Eurostars Project MAS 2020. He is also an EU Coordinator of HORIZON 2020 FETOPEN Science Excellence Project B-CRATOS, a visionary project in man machine interface. He has been invited at the Swedish Royal Academy of Sciences to present his work on noninvasive physiological sensing. He is also a Project Coordinator for Indo–Swedish Vinnova Project BDAS and Swedish part of the bilateral (The Netherlands and Sweden) Horizon 2020 Eurostars Project COMFORT. He is the author or coauthor of more than 180 publications, including journals and conferences and has three patents. His thesis topic was "Electromagnetic modeling of human tissues and its application on the interaction between antenna and human body in the BAN context," two Ph.D. students graduated in 2019 under his supervision. He has received Carl Trygger and Olle Engqvist fundings for his postdoctoral research. His current research interests include designing of wearable antennas, BMD sensors, microwave phantoms, dielectric characterization, bionics, mechatronics, non-invasive diagnostics, point of care sensors for physiological monitoring, clinical trials, animal trials, and on body microwave communication. He has pioneered the Fat—Intra Body Communication Technique. He was a recipient of UGCRFSMS fellowship from Indian Government and EGIDE Eiffel grant for excellence from French Research Ministry, in 2006 and 2008, respectively, and the Swedish Research Agency, Vetenskapsrådet's (VR) Project grant 2017 for his project on "A Novel Modality for Osteodiagnosis" and the Attractive Innovation Project 2020 Award from Uppsala University Innovation. He is the Regular Sessions Chair and a Convened Session Organizer of EuCAP. He is an Editorial Board Member of IET Electronics Letters and Frontiers in Communication. He has been a Board Member with the Department of Electrical Engineering, since January 2020.